Letter

Universal clusters in quasi-two-dimensional ultracold Fermi mixtures

Ruijin Liu [1], Tingting Shi [2], Matteo Zaccanti,[3,4] and Xiaoling Cui[2,*]

[1]Institute of Theoretical Physics, University of Science and Technology Beijing, Beijing 100083, China

[2]Beijing National Laboratory for Condensed Matter Physics, Institute of Physics, Chinese Academy of Sciences, Beijing, 100190, China

[3]Istituto Nazionale di Ottica del Consiglio Nazionale delle Ricerche (CNR-INO), 50019 Sesto Fiorentino, Italy

[4]European Laboratory for Non-Linear Spectroscopy (LENS), Università di Firenze, 50019 Sesto Fiorentino, Italy

(Received 4 August 2024; accepted 16 September 2024; published 4 October 2024)

We study universal clusters in quasi-two-dimensions (q2D) that consist of a light (L) atom interacting with two or three heavy (H) identical fermions, forming the trimer or tetramer bound state. The axial confinement in q2D is shown to lift the threefold degeneracy of three-dimensional trimer (tetramer) in p-wave channel and uniquely select the ground state with magnetic angular momentum $|m| = 1$ ($m = 0$). By varying the interaction or confinement strength, we explore the dimensional crossover of these clusters from 3D to 2D, characterized by a gradual change of critical H-L mass ratio for their emergence and momentum-space distribution. Importantly, we find that a finite effective range will not alter their critical mass ratios in the weak coupling regime. There, we establish an effective 2D model to quantitatively reproduce the properties of q2D clusters, and further identify the optimal interaction strengths for their detections in experiments. Our results suggest a promising prospect for observing universal clusters and associated high-order correlation effects in realistic q2D ultracold Fermi mixtures.

DOI: 10.1103/PhysRevResearch.6.L042004

The knowledge of few-body bound states is essential for tackling complex many-body problems, since their emergence is usually a precursor of dominant few-body correlation in according many-body systems. In the study of few-body physics, dilute atomic gases have provided an ideal platform and various few-body clusters have been revealed therein [1,2]. Among all of them, the $(1 + N)$ system that consists of a light (L) atom interacting with N heavy (H) identical fermions emerges as a rare and fascinating case to host universal cluster bound states [3–11]. Unlike the Efimov states [5,12,13], these universal clusters are insensitive to short-range details of H-L interactions and are expected to be collisionally stable. Physically, their formation can be attributed to the light-atom-mediated long-range attraction between heavy fermions [3,14], and only beyond a critical heavy-light mass ratio η_c such attraction can overcome the Pauli pressure of heavy fermions to support such universal binding. Up to date, the critical η_c have been successfully extracted in three dimensions (3D) [3–5] and 2D [6–8] for $N \leqslant 4$ and in 1D [9–11] for $N \leqslant 5$. The existence of such universal clusters has been shown to intrigue exotic new many-body phases of fermionic matter [15–20]. A particularly interesting case is 2D, where η_c for $(1 + N)$ clusters are sufficiently low to be accessible by currently available ultracold Fermi mixtures [21] such as ^{40}K - ^{6}Li [22–24], ^{161}Dy - ^{40}K [25,26], and ^{53}Cr - ^{6}Li [27–30], and where quartet superfluid may emerge [19]: a high-order superfluid state beyond the conventional pairing paradigm in two-component fermion systems.

The experimental detection of two-dimensional universal clusters in ultracold gases yet requires two key issues to be resolved. First, in ultracold systems there is no pure 2D, but just quasi-2D (q2D) under strong axial confinement. How clusters behave in q2D is thus an important question for their practical detection, as previously addressed for Efimov states [31,32]. In particular, a conceptual challenge here is to understand the structural change of universal clusters along the three- to two-dimensional crossover: in 3D, the ground state trimer and tetramer are known to be threefold degenerate in the p-wave channel [3–5], whereas in 2D such a degeneracy vanishes and the clusters are associated to different angular momenta [6–8]. In this context, the quasi-two-dimensional study is essential to bridge distinct few-body physics in different geometries. The second key question concerns the finite effective range, which has been shown to affect the cluster energy in 3D [4,5]. Here this aspect is crucial for currently available Fermi mixtures [22–30] that generally have narrow Feshbach resonances with large effective range R^* (much larger than van der Walls length [34]). Testing the robustness of quasi-two-dimensional clusters against a large R^* is thus fundamental to their realistic detections.

In this work, we positively address these two questions by exactly solving the $(1 + N)$ problems in q2D with $N = 2$ (trimer) and $N = 3$ (tetramer). By considering either a harmonic or uniform axial confinement, we unveil the general structure of quasi-two-dimensional clusters as well as their connection to pure three-dimensional and two-dimensional ones upon changing the confinement or interaction strength. As shown in Fig. 1 for $R^* = 0$, starting

*Contact author: xlcui@iphy.ac.cn

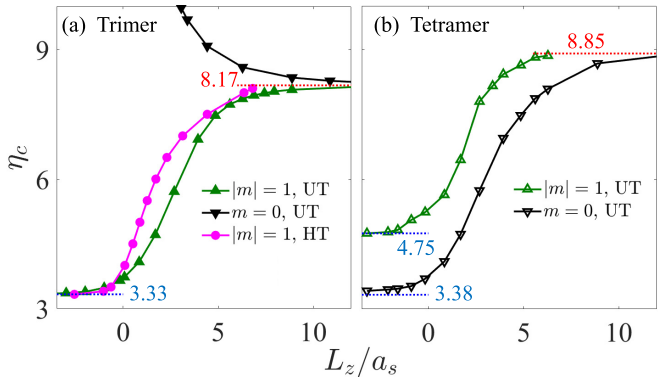

FIG. 1. Critical heavy-light mass ratios η_c for (a) universal trimer and (b) tetramer with different magnetic angular momenta $m = 0, \pm 1$ in quasi-2D. In (a) we consider two axial confinements as harmonic trap (HT) [33] and uniform trap (UT), and in (b) we only consider UT. L_z is the axial trap length, and a_s is the three-dimensional s-wave scattering length (assuming $R^* = 0$). Horizontal red and blue lines mark η_c in our numerics for various clusters in pure 3D and 2D, which were previously studied in Refs. [3–8].

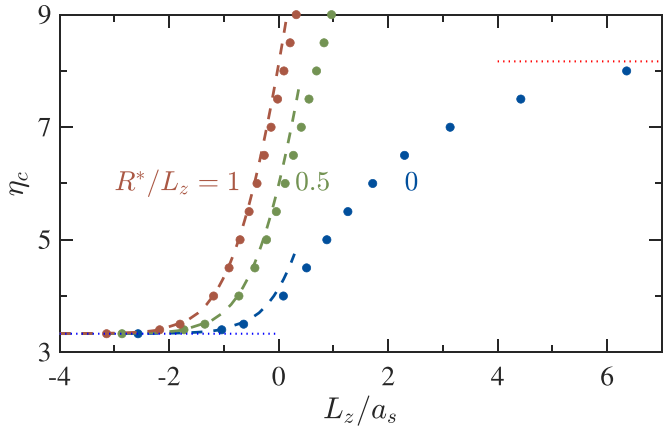

FIG. 3. Critical mass ratios η_c of ground-state trimer ($|m| = 1$) at different effective range $R^*/L_z = 0,\ 0.5,\ 1$. Here we take the axial harmonic trap. Discrete points are exact numerical results and dashed lines are theoretical predictions from the effective two-dimensional model. Horizontal red and blue dotted lines show η_c for pure 3D [3] and 2D [6].

from three-dimensional trimer [3] and tetramer [4,5], which are both threefold degenerate with angular momenta $L = 1$, $m = 0, \pm 1$, the application of an axial trap lifts such degeneracy and leads to a splitting of η_c between $m = 0$ and $m = \pm 1$ channels. The resulting ground state of quasi-two-dimensional trimer (tetramer) is uniquely associated with $|m| = 1$ ($m = 0$), well connecting to pure two-dimensional case [6–8]. Besides η_c, the crossover of these clusters can also be inferred from their momentum distributions (Fig. 2). Importantly, a finite R^* is found to hardly affect η_c in the weak coupling regime (Fig. 3), suggesting the robustness of these clusters even under large R^*. Focusing on this regime, we establish an effective two-dimensional model to quantitatively reproduce the properties of these clusters, and further extract the optimal parameters for their experimental detections (Fig. 4). By identifying a feasible route towards the observation of universal clusters, this work paves the way for future exploration of novel few- and many-body phases in ultracold fermionic matter.

We start from the Hamiltonian of $(1 + N)$-body system in q2D ($\hbar = 1$):

$$H = \left(-\frac{\nabla^2_{\mathbf{r}_l}}{2m_l} + V_l(z_l)\right) + \sum_{i=1}^{N}\left(-\frac{\nabla^2_{\mathbf{r}_{h,i}}}{2m_h} + V_h(z_{h,i})\right) + g\sum_{i=1}^{N}\delta(\mathbf{r}_l - \mathbf{r}_{h,i}). \quad (1)$$

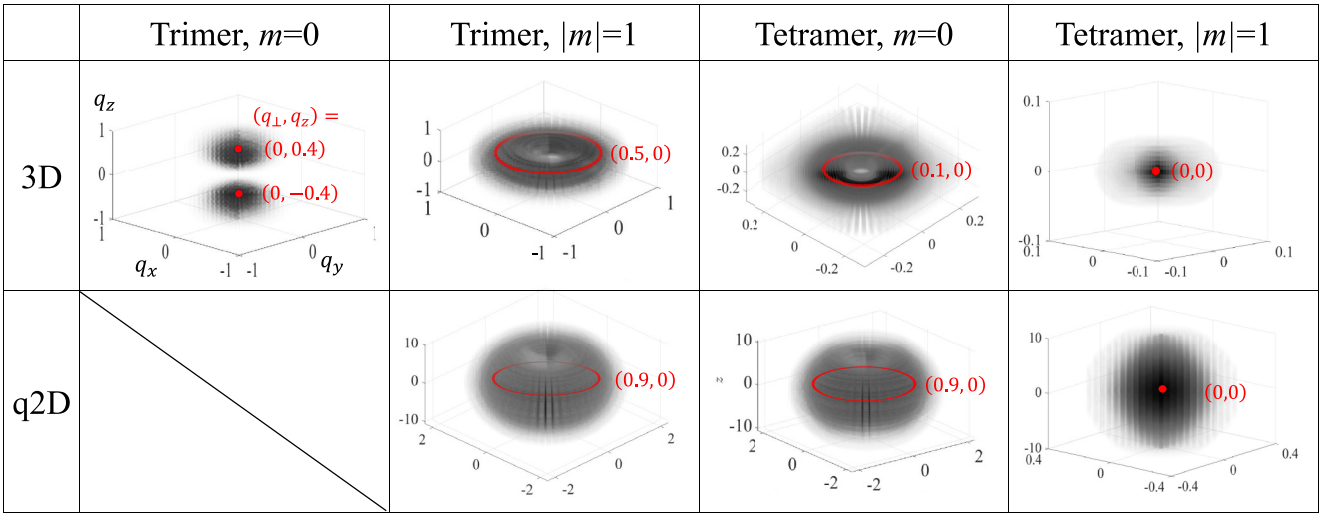

FIG. 2. Momentum distribution of heavy fermions ($n_h(\mathbf{q})$) for different clusters at $\eta = 9$ in 3D and q2D. The values of n_h increase as the color changes from white to black. Red color denotes the location of maximal n_h, with coordinate $(q_\perp = \sqrt{q_x^2 + q_y^2}, q_z)$ shown accordingly. For q2D, we have considered the axial harmonic trap with $L_z/a_s = -1.6$. The tetramer distributions in q2D are from the effective two-dimensional model assuming a frozen motion along z (at the lowest harmonic level), and all other distributions are exact results. The momentum unit is $1/\bar{a}$, with $\bar{a} = (2m_r|\epsilon_2|)^{-1/2}$ the typical dimer size.

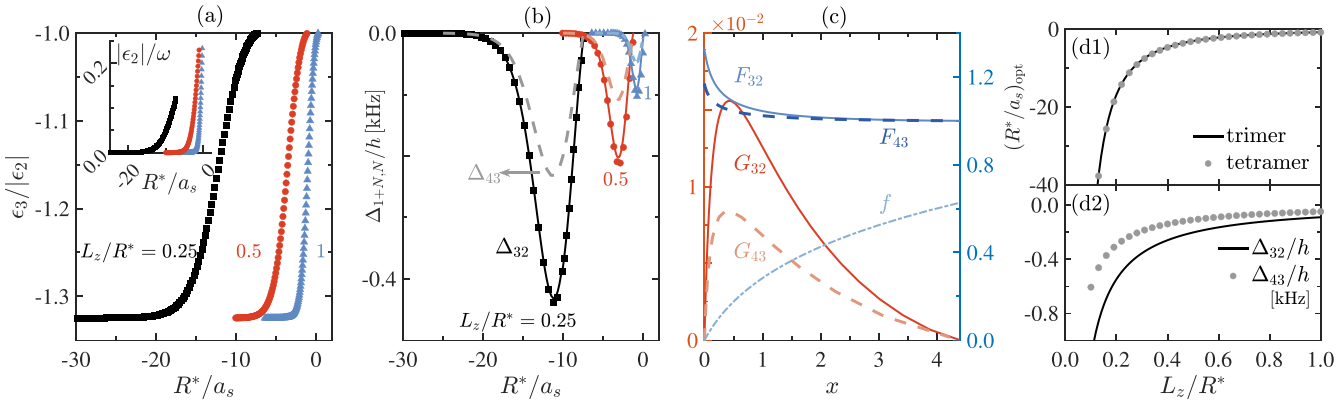

FIG. 4. Universal trimer and tetramer in realistic q2D ^{6}Li-^{53}Cr system ($R^* \simeq 6000a_0$) under an axial harmonic trap. (a) shows $\epsilon_3/|\epsilon_2|$ as a function of R^*/a_s for different L_z/R^*. Inset shows the corresponding $|\epsilon_2|/\omega$. (b) shows $\Delta_{1+N,N} = \epsilon_{1+N} - \epsilon_N$ ($N = 2, 3$) as functions of R^*/a_s for different L_z/R^*. Discrete points are exact numerical results and continuous lines are predictions from the effective two-dimensional model. (c) shows functions $\{f,\ F_{32},\ F_{43}\}$ and $\{G_{32},\ G_{43}\}$. (d1), (d2) show, respectively, the optimal R^*/a_s and the deepest $\{\Delta_{32},\ \Delta_{43}\}$ computed from the effective two-dimensional model as functions of L_z/R^*.

Here $\mathbf{r}_l$ and m_l ($\mathbf{r}_{h,i}$ and m_h) are the coordinate and mass of the light atom (the ith heavy fermion). V_σ ($\sigma = l, h$) is the axial trapping potential, and we will consider two types of V: harmonic trap (HT) $V_\sigma(z) = m_\sigma\omega^2 z_\sigma^2/2$ with typical length $L_z = 1/\sqrt{2m_r\omega}$ ($m_r = m_h m_l/(m_h + m_l)$ is reduced mass), and uniform trap (UT) with finite length L_z and periodic boundary condition. The bare coupling g is renormalized via $1/g = m_r/(2\pi a_s) - 1/V\sum_{\mathbf{Q}} 2m_r/\mathbf{Q}^2$, with a_s the three-dimensional s-wave scattering length. A finite effective range ($R^* > 0$) can be incorporated in the energy-dependent scattering length [34]

$$a_s^{-1}(E) = a_s^{-1} + R^*(2m_r E), \tag{2}$$

with E denoting the energy of two colliding atoms in the center-of-mass (CoM) frame.

We now exactly solve the $(1 + N)$ problems in q2D. For $(1 + 1)$ dimer, by separating the CoM from relative motions we obtain [35] $F(E_2) = 0$, where E_2 is the energy of relative motion and

$$F(E) = \frac{m_r}{2\pi a_s(E)} - \frac{1}{V}\sum_{\mathbf{Q}}\frac{2m_r}{\mathbf{Q}^2} - \frac{1}{S}\sum_{m,\mathbf{p}}\frac{|\phi_m(0)|^2}{E - \epsilon_m^z - \epsilon_{\mathbf{p}}^\perp}. \tag{3}$$

Here $\phi_m(z)$ is the mth eigenstate of relative motion along z with energy ϵ_m^z, $\mathbf{k}$ is the transverse momentum with energy $\epsilon_{\mathbf{k}}^\perp = \mathbf{k}^2/(2m_r)$, and S is the transverse area. The dimer binding energy is given by $\epsilon_2 = E_2 - \epsilon_{m=0}^z$.

When solving the cluster bound states, we use different methods for different axial confinements. For HT, we solve the $(1 + 2)$ trimer by separating out the CoM motion as done previously [36]. Introducing the relative coordinates $\mathbf{r} = \mathbf{r}_{h,1} - \mathbf{r}_l$ and $\boldsymbol{\rho} = \mathbf{r}_{h,2} - (m_l\mathbf{r}_l + m_h\mathbf{r}_{h,1})/(m_l + m_h)$, and imposing the Schrödinger equation $H(\mathbf{r}, \boldsymbol{\rho})\Psi_3 = E_3\Psi_3$, we arrive at [35]

$$F\left(E_3 - \epsilon_n^{z;\rho} - \epsilon_{\mathbf{k}}^{\perp;\rho}\right) f_{n,\mathbf{k}} = -\frac{1}{S}\sum_{n',\mathbf{k}'} A_{n\mathbf{k};n'\mathbf{k}'} f_{n',\mathbf{k}'}, \tag{4}$$

Here $\epsilon_{\mathbf{k}}^{\perp;\rho} = \mathbf{k}^2/(2m_\rho)$ $[m_\rho = m_h(m_h + m_l)/(2m_h + m_l)]$, $\epsilon_n^{z;\rho} = (n + 1/2)\omega$, and $A_{n\mathbf{k};n'\mathbf{k}'}$ is the element produced by the Green's function when exchanging $\mathbf{r}_{h,1} \leftrightarrow \mathbf{r}_{h,2}$. Physically, $f_{n,\mathbf{k}}$ is the Fourier transformation of atom-dimer wave function. The trimer binding energy is then given by $\epsilon_3 = E_3 - \omega$.

For UT, the situation can be greatly simplified since the eigenstates along z are still plane waves. In this case, we are able to solve both $(1 + 2)$ trimer and $(1 + 3)$ tetramer. Introducing n and $\mathbf{k}$ as the indices of longitudinal and transverse momenta, which gives the single-particle energy $\epsilon_{n\mathbf{k}}^\sigma = [n^2(2\pi/L_z)^2 + \mathbf{k}^2]/(2m_\sigma)$ ($\sigma = l, h$), we obtain the following coupled equations [35]:

$$f_{n_2\mathbf{k}_2\ldots n_N\mathbf{k}_N}\left(\frac{m_r}{2\pi a_s(\mathcal{E})} - \frac{1}{V}\sum_{\mathbf{Q}}\frac{2m_r}{\mathbf{Q}^2} + \sum_{n\mathbf{k}}\frac{(L_z S)^{-1}}{E_{n\mathbf{k}n_2\mathbf{k}_2\ldots n_N\mathbf{k}_N}}\right)$$
$$= (L_z S)^{-1}\sum_{\mathbf{k}}\frac{\sum_{i=2}^N f_{n_2\mathbf{k}_2\ldots n_i\mathbf{k}_i\ldots n_N\mathbf{k}_N}\delta_{nn_i}\delta_{\mathbf{k}\mathbf{k}_i}}{E_{n\mathbf{k}n_2\mathbf{k}_2\ldots n_N\mathbf{k}_N}}, \tag{5}$$

with $E_{n_1\mathbf{k}_1 n_2\mathbf{k}_2\ldots n_N\mathbf{k}_N} = -E_{1+N} + \epsilon^l_{-n_1\ldots-n_N,-\mathbf{k}_1\ldots-\mathbf{k}_N} + \sum_{i=1}^N \epsilon^h_{n_i\mathbf{k}_i}$ and $\mathcal{E} = E_{1+N} - [(n_2\ldots + n_N)^2(2\pi/L_z)^2 + (\mathbf{k}_2\ldots + \mathbf{k}_N)^2]/[2(m_h + m_l)] - \sum_{i=2}^N \epsilon^h_{n_i\mathbf{k}_i}$. Here E_{1+N} directly gives the binding energy ϵ_{1+N}. After determining f functions from Eqs. (4), (5), the cluster wave functions can also be obtained [35].

In our numerics, we have simplified Eqs. (4), (5) by noting that the system preserves the total magnetic angular momentum $m_{\rm tot} \equiv m$. It then follows that Eqs. (4), (5) can be decomposed into different m sectors, and each m sector can be solved separately [35]. This also allows us to sort out the intrinsic relation between quasi-two-dimensional clusters and pure three-/two-dimensional ones, as discussed below.

Assuming $R^* = 0$, in Fig. 1 we show the critical mass ratios ($\eta_c = m_h/m_l$) for the emergence of trimer and tetramer in q2D, as given by the conditions $\epsilon_3 = \epsilon_2$ and $\epsilon_4 = \epsilon_3$, respectively [35]. In the limit $L_z/a_s \to +\infty$, η_c approaches $\eta_c^{\rm 3D}$ (horizontal red lines) for three-dimensional trimers [3] and tetramers [4,5], which all belong to the p-wave channel with threefold degeneracy ($L = 1$ and $|m| = 0, 1$). However, as L_z/a_s becomes finite, η_c starts to split between $|m| = 0$

and 1, owing to the fact that the rotating symmetry is partly broken by the axial trap and L is no longer a good number. The resulting ground state (with a lower η_c) is solely associated with $|m| = 1$ for trimer and $m = 0$ for tetramer. As $L_z/a_s \to -\infty$, η_c of various states continuously decrease and finally saturate at pure 2D values η_c^{2D} (horizontal blue lines), as previously studied in Refs. [6–8]. The picture in Fig. 1 reveals the intimate connection of quasi-two-dimensional clusters to their three-/two-dimensional counterparts, and this picture is robust against the specific choice of axial confinement, as seen from the results of HT and UT in Fig. 1(a).

Beside η_c, the dimensional crossover of quasi-two-dimensional clusters can be reflected in the momentum distribution of heavy fermions, $n_h(\mathbf{q})$. In Fig. 2 we assume $\eta = 9$ and show $n_h(\mathbf{q})$ for various clusters along the 3D to 2D crossover. Notably, different m states feature completely different $n_h(\mathbf{q})$. For three-dimensional trimers, their angular dependence follows $n_h(\mathbf{q}) \propto |Y_{1m}(\Omega_\mathbf{q})|^2$ for each m sector. As a result, the maxima of $n_h(\mathbf{q})$ locate along z axis for $m = 0$, while laying in xy plane for $m = \pm 1$, see Fig. 2. For three-dimensional tetramers, $m = 0$ and $m = \pm 1$ states also exhibit distinct $n_h(\mathbf{q})$, whose maxima respectively locate in xy plane with a finite $|\mathbf{q}_\perp|$ and at the origin $\mathbf{q} = 0$. When crossing over to the two-dimensional regime, the general structures of $n_h(\mathbf{q})$ do not change, except that the distributions along z are frozen at the lowest axial mode [37]. The unchanged structure also explains why $m = 0$ trimer disappears in 2D, due to the incompatible z distributions between three-dimensional and two-dimensional limits, as also seen from the tendency $\eta_c \to \infty$ in 2D limit in Fig. 1. In contrast, all other clusters inherit similar distributions from 3D to 2D and thus can all survive in q2D. Furthermore, similar to the two-dimensional case [8], the high-order correlations in quasi-two-dimensional clusters can induce crystalline patterns in their two-body density distributions [35].

We now move to the finite range effect. Similar to three-dimensional clusters [4,5], we find that in q2D a finite R^* generally increases η_c and disfavors cluster formation. However, it can hardly affect η_c in the effective two-dimensional regime ($L_z/a_s \ll -1$). As shown in Fig. 3 for $|m| = 1$ trimer, as $L_z/a_s \to -\infty$, all η_c for different R^*/L_z saturate to η_c^{2D}, the critical value in pure 2D with $R^* = 0$ [6]. We have numerically checked that the saturation $\eta_c \to \eta_c^{2D}$ universally applies to clusters under UT [35]. This remarkable behavior suggests the detectability of these clusters in realistic quasi-two-dimensional systems even with large R^*. For specific ^{40}K-^{6}Li mixture, we note that the critical boundaries $\{R^*/L_z, L_z/a_s\}$ in Fig. 3 agree with those in Ref. [36].

To understand above behavior, we construct an effective two-dimensional model by utilizing the reduced scattering length a_{2D} and effective range R_{2D}, which enters the two-dimensional scattering amplitude as:

$$T_{2D}(k) = \frac{2\pi}{m_r}\left[-\ln\left(k^2 a_{2D}^2\right) + i\pi + R_{2D}k^2\right]^{-1}, \tag{6}$$

here k is the relative collision momentum. For HT, the reduced two-dimensional parameters were derived previously in Refs. [7,38–40], and here we obtain [35]

$$a_{2D} = \sqrt{\frac{\pi}{0.905}} L_z \exp\left[-\sqrt{\frac{\pi}{2}}\left(\frac{L_z}{a_s} + \frac{R^*}{2L_z}\right)\right];$$
$$R_{2D} = \sqrt{2\pi} R^* L_z + (\ln 2) L_z^2, \tag{7}$$

$\{a_{2D}, R_{2D}\}$ for the case of UT are presented in Ref. [35].

Now the universal trend $\eta_c \to \eta_c^{2D}$ for any R^* in effective two-dimensional regime can be understood. From scaling analysis, in this regime η_c only depends on a single parameter R_{2D}/a_{2D}^2, which approaches zero as $L_z/a_s \to -\infty$ since $a_{2D} \to \infty$ while R_{2D} is finite. As a result, the finite range plays no effect here, and η_c^{2D} is recovered for all R^* (or R_{2D}). On the other hand, in the same regime the absolute binding energies of these clusters can be very small, since all $|\epsilon_n| \propto a_{2D}^{-2} \to 0$. Therefore, it is important to examine how deep the clusters can be bound under realistic R^*, L_z, and a_s, from which one can identify the optimal parameters for their practical detections.

To do that, we have considered the realistic ^{6}Li-^{53}Cr system with a large $R^* \simeq 6000 a_0$ [27–30] and calculated the absolute binding energies of q2D clusters under HT. Figure 4(a) shows that as decreasing L_z, the range of R^*/a_s for trimer formation ($\epsilon_3/|\epsilon_2| < -1$) expands from a narrow region near resonance to a considerably broader one on $a_s < 0$ side. Figure 4(b) further shows $\Delta_{32} \equiv \epsilon_3 - \epsilon_2$, which displays a nonmonotonic dependence on R^*/a_s. For tighter axial trap (smaller L_z), the maximum of $|\Delta_{32}|$ becomes larger and its location moves towards weaker coupling, i.e., more negative R^*/a_s.

To understand these behaviors, we exploit the effective two-dimensional model to solve the $(1+N)$ problem [35]:

$$f_{\mathbf{k}_2\ldots\mathbf{k}_N}\left(-\sum_\mathbf{k}\frac{2m_r}{\mathbf{k}^2 + a_{2D}^{-2}} + \frac{Sm_r^2}{\pi}R_{2D}\mathcal{E} + \sum_\mathbf{k}\frac{1}{E_{\mathbf{k}\mathbf{k}_2\ldots\mathbf{k}_N}}\right)$$
$$= \sum_\mathbf{k}\frac{\sum_{i=2}^N f_{\mathbf{k}_2\ldots\mathbf{k}_{i-1}\mathbf{k}_i\mathbf{k}_{i+1}\ldots\mathbf{k}_N}\delta_{\mathbf{k}\mathbf{k}_i}}{E_{\mathbf{k}\mathbf{k}_2\ldots\mathbf{k}_N}}, \tag{8}$$

with $E_{\mathbf{k}_1\mathbf{k}_2\ldots\mathbf{k}_N} = -\epsilon_{1+N} + \epsilon^l_{-\mathbf{k}_1\ldots-\mathbf{k}_N} + \sum_{i=1}^N \epsilon^h_{\mathbf{k}_i}$ and $\mathcal{E} = \epsilon_{1+N} - (\mathbf{k}_2\ldots+\mathbf{k}_N)^2/[2(m_h+m_l)] - \sum_{i=2}^N \epsilon^h_{\mathbf{k}_i}$. Utilizing $\{a_{2D}, R_{2D}\}$ in Eq. (7), we find Eq. (8) yield Δ_{32} in very good agreement with exact results for $L_z/R^* \lesssim 1$, suggesting the validity of this model even for moderate confinement [35]. We further exploit this model to compute $\Delta_{43} \equiv \epsilon_4 - \epsilon_3$, and it shows a similar nonmonotonic behavior as Δ_{32}, see Fig. 4(b). From the effective two-dimensional model, it is clear that such nonmonotonicity is due to the enhanced finite-range effect, i.e., the growing R_{2D}/a_{2D}^2 as $1/a_s$ is tuned to strong couplings.

We now identify the optimal interaction strength for detecting $(1+N)$ clusters and their associated deepest $\Delta_{1+N,N}$. Based on the effective 2D model, we introduce a dimensionless parameter

$$x = R_{2D}/a_{2D}^2, \tag{9}$$

and express ϵ_2 and ϵ_3 as

$$\epsilon_2 = -\frac{1}{m_r R_{2D}} f(x); \quad \epsilon_3 = \epsilon_2 F_{32}(\eta, x). \tag{10}$$

Both f and F_{32} are dimensionless functions and can be obtained from Eqs. (6), (8). Then we have $\Delta_{32} = -1/(m_r R_{2D}) G_{32}(\eta, x)$, with

$$G_{32}(\eta, x) = [F_{32}(\eta, x) - 1] f(x). \tag{11}$$

Similarly, for the tetramer we can define $F_{43}(\eta, x) \equiv \epsilon_4/\epsilon_3$ and $\Delta_{43} = -1/(m_r R_{2D}) G_{43}(\eta, x)$, with

$$G_{43}(\eta, x) = [F_{43}(\eta, x) - 1] F_{32}(\eta, x) f(x). \tag{12}$$

In Fig. 4(c) we show the functions f, $F_{1+N,N}$ and $G_{1+N,N}$ ($N = 2, 3$) for Li-Cr system. By increasing x from 0 (two-dimensional limit), f monotonically increases while $F_{1+N,N}$ decreases from a finite value down to 1, where $(1 + N)$ cluster vanishes. As a result, $G_{1+N,N}$ depends nonmonotonically on x, and its maximum occurs at x_m, which is a universal constant solely relying on η. Here x_m and its according $G_{1+N,N}$ respectively give the optimal interaction strength and the deepest binding energy for $(1 + N)$ cluster. Recalling Eq. (7), we finally obtain the optimal R^*/a_s and its associated $\Delta_{1+N,N}$ for given L_z/R^*, see Figs. 4(d1), 4(d2). One can see that the optimal condition to detect $\Delta_{1+N,N}$ is the weak coupling regime with strong axial confinement. For instance, at $L_z = 0.2R^*$, the deepest energy detunings for trimer and tetramer can be as large as $|\Delta_{32}| \sim 550$ Hz and $|\Delta_{43}| \sim 300$ Hz, respectively. Interestingly, the optimal R^*/a_s that maximize $|\Delta_{32}|$ and $|\Delta_{43}|$ are very close and almost indistinguishable: this can be attributed to the intimate relation between two-dimensional trimer and tetramer [8], as also inferred by their very close η_c^{2D} [6,8].

In summary, we have revealed the basic structure of universal $(1 + N)$ clusters along the 3D-2D crossover, as classified by different angular momenta and manifested in the evolution of critical mass ratios and momentum distributions. Importantly, it is shown that a finite effective range does not affect the critical mass ratio for cluster formation in the effective two-dimensional limit, but leads to a nonmonotonic binding energy as changing coupling strength. The optimal coupling and deepest binding energy have been successfully extracted from an effective two-dimensional model, offering an essential guide for future detection of these clusters and associated high-order correlation effects in currently available ultracold Fermi mixtures.

We expect that the effective two-dimensional model established here can serve as a convenient tool for tackling general quasi-two-dimensional problems with an arbitrary axial confinement. For a general case, our analyses on finite range effect and optimal detection conditions [Eqs. (9)–(12)] are universally applicable once the reduced $\{a_{2D}, R_{2D}\}$ are given. Finally, we remark that the disappearance of ground-state trimer (tetramer) at critical η_c (or at critical R^*/L_z and L_z/a_s for given η) corresponds to the cluster state hitting the atom-dimer (atom-trimer) scattering threshold. Beyond such a critical boundary, the trimer (tetramer) turns into a p-wave resonance between one dimer (trimer) and a heavy fermion [36,41]. This opens a new avenue to explore p-wave physics in effective Bose-Fermi or Fermi-Fermi mixtures.

The work is supported by the National Natural Science Foundation of China (No. 12074419, No. 12134015), the Strategic Priority Research Program of Chinese Academy of Sciences (XDB33000000). T.S. acknowledges support from the Postdoctoral Fellowship Program of CPSF (No. GZC20232945). R.L. acknowledges support from the National Natural Science Foundation of China (No. 12404316), the Fundamental Research Funds for the Central Universities (No. FRF-TP-24-040A) and the 2023 Fund for Fostering Young Scholars of the School of Mathematics and Physics, USTB (No. FRF-BR-23-01B).

[1] Chris H. Greene, P. Giannakeas, and J. Pérez-Ríos, Universal few-body physics and cluster formation, Rev. Mod. Phys. **89**, 035006 (2017).
[2] P. Naidon and S. Endo, Efimov physics: a review, Rep. Prog. Phys. **80**, 056001 (2017).
[3] O. I. Kartavtsev and A. V. Malykh, Low-energy three-body dynamics in binary quantum gases, J. Phys. B **40**, 1429 (2007).
[4] D. Blume, Universal four-body states in heavy-light mixtures with a positive scattering length, Phys. Rev. Lett. **109**, 230404 (2012).
[5] B. Bazak and D. S. Petrov, Five-Body efimov effect and universal pentamer in fermionic mixtures, Phys. Rev. Lett. **118**, 083002 (2017).
[6] L. Pricoupenko and P. Pedri, Universal (1+2)-body bound states in planar atomic waveguides, Phys. Rev. A **82**, 033625 (2010).
[7] J. Levinsen and M. M. Parish, Bound states in a quasi-two-dimensional fermi Gas, Phys. Rev. Lett. **110**, 055304 (2013).
[8] R. Liu, C. Peng, and X. Cui, Universal tetramer and pentamer in two-dimensional fermionic mixtures, Phys. Rev. Lett. **129**, 073401 (2022).
[9] O. I. Kartavtsev, A. V. Malykh, and S. A. Sofianos, Bound states and scattering lengths of three two- component particles with zero-range interactions under one-dimensional confinement, J. Exp. Theor. Phys. **108**, 365 (2009).
[10] N. P. Mehta, Born-Oppenheimer study of two-component few-particle systems under one-dimensional confinement, Phys. Rev. A **89**, 052706 (2014).
[11] A. Tononi, J. Givois, and D. S. Petrov, Binding of heavy fermions by a single light atom in one dimension, Phys. Rev. A **106**, L011302 (2022).
[12] V. N. Efimov, Energy levels of three resonantly interacting particles, Nucl. Phys. A **210**, 157 (1973).
[13] Y. Castin, C. Mora, and L. Pricoupenko, Four-Body efimov effect for three fermions and a lighter particle, Phys. Rev. Lett. **105**, 223201 (2010).
[14] A. C. Fonseca, E. F. Redish, and P. E. Shanley, Efimov effect in an analytically solvable model, Nucl. Phys. A **320**, 273 (1979).
[15] C. J. M. Mathy, M. M. Parish, and D. A. Huse, Trimers, molecules, and polarons in mass-imbalanced atomic Fermi gases, Phys. Rev. Lett. **106**, 166404 (2011).

[16] M. M. Parish and J. Levinsen, Highly polarized Fermi gases in two dimensions, Phys. Rev. A **87**, 033616 (2013).
[17] S. Endo, A. M. García-García, and P. Naidon, Universal clusters as building blocks of stable quantum matter, Phys. Rev. A **93**, 053611 (2016).
[18] R. Liu, C. Peng, and X. Cui, Emergence of crystalline few-body correlations in mass-imbalanced fermi polarons, Cell Reports Phys. Sci. **3**, 100993 (2022).
[19] R. Liu, W. Wang, and X. Cui, Quartet superfluid in two-dimensional mass-imbalanced fermi mixtures, Phys. Rev. Lett. **131**, 193401 (2023).
[20] R. Li, J. von Milczewski, A. Imamoglu, R. Ołdziejewski, and R. Schmidt, Impurity-induced pairing in two-dimensional Fermi gases, Phys. Rev. B **107**, 155135 (2023).
[21] Here we do not consider the Bose-Fermi mixture, since in this system there are additional Efimov-type clusters formed by a fermion and a few bosons.
[22] M. Taglieber, A.-C. Voigt, T. Aoki, T. W. Hänsch, and K. Dieckmann, Quantum degenerate two-species fermi-fermi mixture coexisting with a Bose-Einstein condensate, Phys. Rev. Lett. **100**, 010401 (2008).
[23] E. Wille, F. M. Spiegelhalder, G. Kerner, D. Naik, A. Trenkwalder, G. Hendl, F. Schreck, R. Grimm, T. G. Tiecke, J. T. M. Walraven, S. J. J. M. F. Kokkelmans, E. Tiesinga, and P. S. Julienne, Exploring an ultracold fermi-fermi mixture: Interspecies feshbach resonances and scattering properties of ^{6}Li and ^{40}K, Phys. Rev. Lett. **100**, 053201 (2008).
[24] A.-C. Voigt, M. Taglieber, L. Costa, T. Aoki, W. Wieser, T. W. Hänsch, and K. Dieckmann, Ultracold heteronuclear fermi-fermi molecules, Phys. Rev. Lett. **102**, 020405 (2009).
[25] C. Ravensbergen, V. Corre, E. Soave, M. Kreyer, E. Kirilov, and R. Grimm, Production of a degenerate Fermi-Fermi mixture of dysprosium and potassium atoms, Phys. Rev. A **98**, 063624 (2018).
[26] C. Ravensbergen, E. Soave, V. Corre, M. Kreyer, B. Huang, E. Kirilov, and R. Grimm, Resonantly interacting fermi-fermi mixture of ^{161}Dy and ^{40}K, Phys. Rev. Lett. **124**, 203402 (2020).
[27] E. Neri, A. Ciamei, C. Simonelli, I. Goti, M. Inguscio, A. Trenkwalder, and M. Zaccanti, Realization of a cold mixture of fermionic chromium and lithium atoms, Phys. Rev. A **101**, 063602 (2020).
[28] A. Ciamei, S. Finelli, A. Trenkwalder, M. Inguscio, A. Simoni and M. Zaccanti, Exploring ultracold collisions in ^{6}Li - ^{53}Cr Fermi mixtures: Feshbach resonances and scattering properties of a novel alkali-transition metal system, Phys. Rev. Lett. **129**, 093402 (2022).
[29] A. Ciamei, S. Finelli, A. Cosco, M. Inguscio, A. Trenkwalder, and M. Zaccanti, Double-degenerate Fermi mixtures of ^{6}Li and ^{53}Cr atoms, Phys. Rev. A **106**, 053318 (2022).
[30] S. Finelli, A. Ciamei, B. Restivo, M. Schemmer, A. Cosco, M. Inguscio, A. Trenkwalder, K. Zaremba-Kopczyk, M. Gronowski, M. Tomza, and M. Zaccanti, Ultracold LiCr: A New pathway to quantum gases of paramagnetic polar molecules, PRX Quantum **5**, 020358 (2024).
[31] J. Levinsen, P. Massignan, and M. M. Parish, Efimov trimers under strong confinement, Phys. Rev. X **4**, 031020 (2014).
[32] E. K. Laird, T. Kirk, M. M. Parish, and J. Levinsen, Long-lived trimers in a quasi-two-dimensional Fermi system, Phys. Rev. A **97**, 042711 (2018).
[33] η_c of $m = 0$ trimer under harmonic trap is not shown here given the numerical results are not convergent.
[34] C. Chin, R. Grimm, P. Julienne, and E. Tiesinga, Feshbach resonances in ultracold gases, Rev. Mod. Phys. **82**, 1225 (2010).
[35] See Supplemental Material at http://link.aps.org/supplemental/10.1103/PhysRevResearch.6.L042004 for more details on the derivations of few-body equations and reduced two-dimensional scattering parameters, as well as on the properties of universal clusters under an axial uniform trap.
[36] J. Levinsen, T. G. Tiecke, J. T. M. Walraven, and D. S. Petrov, Atom-dimer scattering and long-lived trimers in fermionic mixtures, Phys. Rev. Lett. **103**, 153202 (2009).
[37] For HT, the typical momentum scale of $n_h(\mathbf{q})$ along z is $q_z \sim (m_r\omega)^{1/2}$, more elongated than the dimer scale $\sim(m_r|\epsilon_2|)^{1/2}$ due to $\omega \gg |\epsilon_2|$ in the effective two-dimensional regime.
[38] D. S. Petrov and G. V. Shlyapnikov, Interatomic collisions in a tightly confined Bose gas, Phys. Rev. A **64**, 012706 (2001).
[39] T. Kirk and M. M. Parish, Three-body correlations in a two-dimensional SU(3) Fermi gas, Phys. Rev. A **96**, 053614 (2017).
[40] H. Hu, B. C. Mulkerin, U. Toniolo, L. He, and X.-J. Liu, Reduced quantum anomaly in a quasi-two-dimensional fermi Superfluid: Significance of the confinement-induced effective range of interactions, Phys. Rev. Lett. **122**, 070401 (2019).
[41] M. Jag, M. Zaccanti, M. Cetina, R. S. Lous, F. Schreck, R. Grimm, D. S. Petrov, and J. Levinsen, Observation of a strong atom-dimer attraction in a mass-imbalanced fermi-fermi mixture, Phys. Rev. Lett. **112**, 075302 (2014).